Available online at www.sciencedirect.com
SCIENCE DIRECT
Polymer 47 (2006) 5505–5512
polymer
www.elsevier.com/locate/polymer

Solution of the growth equation for asymmetric crystal faces

M.A. Shcherbina, G. Ungar *

Department of Engineering Materials, University of Sheffield, Sir Robert Hadfield Building, Mappin Street, Sheffield S1 3JD, UK

Received 29 June 2005; received in revised form 14 November 2005; accepted 20 December 2005
Available online 16 May 2006

Abstract

Most melt-grown and many solution-grown lamellar polymer crystals have curved lateral faces. Mathematical treatments by Mansfield, Point and Villers, and Toda, have provided a satisfactory interpretation of the shape of such crystal faces in terms of nucleation and relatively slow propagation rates of layers of attaching stems. The treatments by these authors, which start with the Frank–Seto growth model, assume that the propagation rates of growth steps to the right (v_r) and to the left of the secondary nucleus (v_l) are equal. However, for many crystal growth faces this is not the case; faces which lack a mirror plane perpendicular to the lamella have $v_r \neq v_l$, resulting in asymmetric curvature. Here, we set up and solve the differential equations and reconstruct the shape of the growth front for the case of asymmetric spreading of steps. The solution is presented for the simple square lattice model. The asymmetric growth front is still described as part of an ellipse, as in the symmetric case, except that the centre of the ellipse is translated parallel to the underlying crystallographic plane in the direction of fast v. In forthcoming publications we will adapt the solution to other 2D Bravais lattices, appropriate to the crystal structures of specific polymers. Thus we will analyze complete habits of polymers such as polyethylene, poly(ethylene oxide), and poly(vinylidene fluoride), whose {110}, {120} and {110} growth faces, respectively, are asymmetric. The results of the present work allow a detail kinetic analysis of any well-developed polymer growth face in terms of the step initiation rate i and the propagation rates v_r and v_l. The present work also quantifies explicitly the deviations from elliptic shape and the substrate edge effects, and discusses when these can be ignored.

Keywords: Crystal growth; Polymer crystallization; Nucleation

1. Introduction

The discovery of rounded crystal edges [1,2] has played an important part in understanding polymer crystallization. For example, it motivated Sadler to propose the rough-surface theory of crystal growth [3,4]. His theory was intended to describe crystallization at higher temperatures, where lateral crystal faces are above their roughening transition temperature T_R. Sadler argued that the fact that the {100} faces in solution-grown polyethylene become curved at high temperatures indicates the presence of the roughening transition. In contrast, {110} faces with somewhat denser packing of surface chains and hence a higher interaction energy would have a higher T_R, hence the {110} faces remain faceted.

However, subsequent detailed studies [5–7] have shown that the curvature of {100} faces in polyethylene can be explained quantitatively by applying Frank's model of initiation and movement of steps [8]. Noticeable curvature occurs when the average step propagation distance is no more than two orders of magnitude larger than the stem width b.

The profile of a {100} face in polyethylene is symmetrical as a consequence of the existence of a mirror plane bisecting the crystal normal to this face and to the crystal layer. However, such symmetry does not apply to {110}, and it is of considerable interest to investigate the shape of curved profiles of these faces if such profiles could be observed. An opportunity to observe the entire profile of curved {110} faces has arisen in very long-chain monodisperse n-alkanes (see below). Thus far, lenticular crystals have been observed in these compounds, with the curved faces being the usual {100} [9]. In fact, pure long alkanes display most if not all the crystal habits encountered in polyethylene [10–12]. Moreover, in contrast to polyethylene, crystal lamellae bounded exclusively by {110} lateral faces can be grown from solution at high temperatures and low supercooling by using monodisperse n-alkanes $C_{162}H_{326}$ and $C_{198}H_{398}$ [13,14]. While faceted non-truncated rhombic crystals grow from octacosane, similarly non-truncated but curved-faced {110}-bounded crystals are formed from 1-phenyldecane and methylanthracene. Thus the revelation of the entire {110} face grown at high temperatures

* Corresponding author. Tel.: +44 114 222 5457; fax: +44 114 222 5923.
E-mail address: g.ungar@sheffield.ac.uk (G. Ungar).

0032-3861/$ - see front matter © 2006 Elsevier Ltd. All rights reserved.
doi:10.1016/j.polymer.2005.12.093

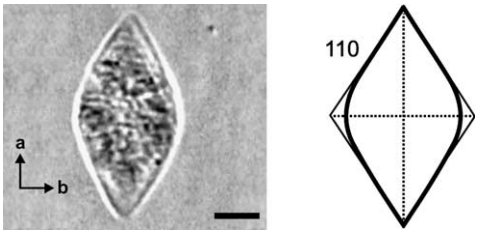

Fig. 1. (left) An '*a*-axis lenticular' crystals of alkane $C_{162}H_{326}$ in 1-phenyldecane grown from an initially 1.0% solution at 99.5 °C. Interference optical micrograph. Bar length 10 μm. (right) Schematic outline of the crystal, indicating the four {110} sectors (from Ref. [13]).

showed that the distinction between {100} and {110} faces in terms of their roughening transition temperatures may not be as significant as Sadler had thought.

However, perhaps a more significant aspect of the observed curved {110} faces is that the curvature is asymmetric, i.e. higher at the obtuse apex than at the acute one [13]. As a consequence, the appearance of the {110}-bounded crystals from the two aromatic solvents is similar to the lenticular crystals of polyethylene grown at high T_c, except that their long dimension is parallel to the crystallographic *a*-axis (Fig. 1) rather than the usual *b*-axis.

In order to rationalize the existence of the new habit it was assumed that the rates of propagation of left and right steps on the growing {110} faces were different [13]. In this paper, we present a mathematical treatment of the profile of a general polymer crystal face whose growth involves different step propagation rates in the two opposing directions. We solve the appropriate differential equation of the secondary nucleation model with moving face boundaries, using a simple square lattice model. The solution is directly applicable only to crystals with a primitive tetragonal unit cell. However, as most polymer crystals do not fall into this category, in subsequent publications we will adapt the model to lattices specific to particular crystalline polymers, construct theoretical shapes of single crystals, and compare them with those observed experimentally. As the full crystal habit is specific to each individual polymer, in this paper we do not discuss the physical nature of the moving boundaries.

2. Summary of the treatment of symmetrical growth profiles

The Seto–Frank treatment [8,15] starts from a surface nucleation event creating a pair of steps. The nucleation rate is i nuclei per unit edge length per time, and the steps travel to the left and right at an average net rate v (in units of length per time). The advance of patches of stems on the substrate is arrested either by collision between left-moving and right-moving steps, or by the patches reaching the end of the crystal. If $l(x,t)$ and $r(x,t)$ are the average densities of left and right steps, respectively, in the vicinity of position x along the substrate of length L, two flux equations must be satisfied:

$$\frac{\partial r}{\partial t} = -v\frac{\partial r}{\partial x} + i - 2vlr \tag{1a}$$

$$\frac{\partial l}{\partial t} = v\frac{\partial l}{\partial x} + i - 2vlr \tag{1b}$$

These describe the local variation in concentration as a result of drift, creation and annihilation processes expressed, respectively, by the first, second and third terms on the right. The mean slope of a growing face is given by

$$\frac{\partial y}{\partial x} = b(l-r) \tag{2}$$

(b is the height of the moving patch).

Assuming that no step enters from outside, the boundary conditions for Eq. (1) are:

$$r\left(\frac{-L}{2}\right) = 0 \tag{3a}$$

$$l\left(\frac{L}{2}\right) = 0 \tag{3b}$$

In real crystal growth the substrate length increases simultaneously with the advance of the growth front. The substrate ends move outward at a net rate h. Thus, (3) is replaced by another set of boundary conditions:

$$r(-ht,t) = 0 \tag{4a}$$

$$l(ht,t) = 0 \tag{4b}$$

In the case of the {100} growth in polyethylene for example, h is determined by G_{110}, the growth rate of the {110} face.

Mansfield [6], Toda [5], and Point and Villers [7] have obtained solutions of the above equations, deriving the growth face profile $y(x,t)$. Such $y(x,t)$ describes adequately the observed [5,16] and simulated [17] shapes of {100} faces of single crystals of polyethylene and, as found recently [10–12], long alkanes. $y(x)$ defines an ellipse if a square lattice is used [6], even though this is not strictly true for very small crystals [7]. The ellipse becomes leaf-shaped when transposed onto a polyethylene-like centered rectangular lattice [18]. The {100} face is given as part of this ellipse when the substrate edge moves at a rate $h<v$, i.e. in the case of a truncated lozenge crystal. On the other hand, if $h>v$, the outer parts of the {100} face are described by straight non-crystallographic faces tangent to the central elliptical section [5,7].

3. Mathematical treatment of the growth profile of asymmetric faces

For asymmetric faces, the above treatment does not apply, as mentioned in the introduction. Fig. 2 illustrates the

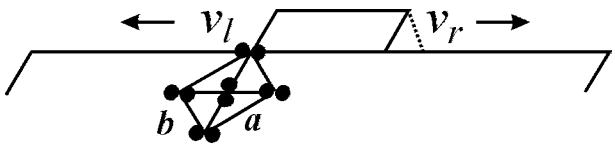

Fig. 2. View along the chain axis of a new molecular layer deposited on a 110 growth face of polyethylene showing the asymmetry of steps. A unit cell is shown for reference.

difference between the 'sharp' (right) and the 'blunt' (left) step on the example of a (110) face of polyethylene. Had the lattice hexagonal symmetry, there would have been no difference between the steps or between their propagation rates; the right and left steps would have been equivalent, both having an angle of 120°. However, in the orthorhombic lattice of polyethylene the two step angles differ by 11°. Similarly, the distance between adjacent chains in the {100} plane (length of the dashed right-hand edge) is shorter than the distance in the {110} plane (length of the left-hand edge). These differences would be expected to produce some difference in either the molecular attachment or detachment rates, or both. With reference to Fig. 2, Eqs. (1) become

$$\frac{\partial r}{\partial t} + v_r \frac{\partial r}{\partial x} = i - (v_r + v_l) l r \tag{5a}$$

$$\frac{\partial l}{\partial t} - v_l \frac{\partial l}{\partial x} = i - (v_r + v_l) l r \tag{5b}$$

In the next section, we present the solution of Eqs. (5a) and (5b) with generalized moving boundary conditions, assuming that for an asymmetric growth face the spreading rates of substrate edges, h_r and h_l, can differ.

$$r(-h_l t, t) = 0 \tag{5c}$$

$$l(h_r t, t) = 0 \tag{5d}$$

As already mentioned, for simplicity we use here a simple square lattice model, which is therefore, not directly applicable to the {110} planes of polyethylene in Fig. 2. A forthcoming paper will deal explicitly with {110} faces of polyethylene and long alkanes [19].

Our procedure for solving the above equations is close to that used by Mansfield for the symmetric growth face. In principle, it is possible to obtain the solution by using the coordinate system where the y-axis moves with a velocity $\delta = (v_r - v_l)/2$; in that case the system of Eqs. (5a) and (5b) becomes the system (1a) and (1b), with $v = (v_r + v_l)/2$. However, the chosen boundary conditions (5c) and (5d) are no longer analogous to those of Mansfield. They now become

$$r((\delta - h_l)t, t) = 0$$

$$l((\delta + h_r)t, t) = 0$$

Since these boundary conditions are asymmetric, the solution is not a trivial one. We therefore, chose to solve Eqs. (5a) and (5b) by another route.

After solving the differential equations in Section 3.1, the resulting functions $r(x,t)$ and $l(x,t)$ will be used in the reconstruction of the shape of the growth face (Section 3.2). The specifics regarding the validity of the approximations used and the choice of integration limits in the reconstruction of the growth front are dealt with in the Appendix A. In subsequent publications, we will adapt the present solutions to different 2D lattices, which correspond to crystal structures of several specific polymers, and compare the calculated habits with the experimentally observed ones. This would provide (a) a test of our model, and (b) allow us to extract kinetic parameters such as i, v_r and v_l for asymmetric faces, which could not be analysed up to now.

3.1. Solution of the differential equations

On the basis of computer simulations [6], we expect that the steady-state solutions are functions of the ratio $u = x/t$ only. Owing to this assumption, total differentials dr and dl are zero on the characteristic line $x = ut$, so that

$$\frac{\partial r}{\partial t} + u \frac{\partial r}{\partial x} = 0 \tag{6a}$$

$$\frac{\partial l}{\partial t} + u \frac{\partial l}{\partial x} = 0 \tag{6b}$$

Subtracting the expressions (6a) and (6b) from (5a) and (5b), respectively, we have:

$$(v_r - u)\frac{dr}{dx} = i - (v_r + v_l) l r \tag{7a}$$

$$-(v_l + u)\frac{dl}{dx} = i - (v_r + v_l) l r \tag{7b}$$

In the steady regime $dx = t_0 du$, so for any definite time

$$\frac{1}{t_0}(v_r - u)\frac{dr}{du} = i - (v_r + v_l) l r \tag{8a}$$

$$-\frac{1}{t_0}(v_l + u)\frac{dl}{du} = i - (v_r + v_l) l r \tag{8b}$$

As the right hand sides of Eqs. (8a) and (8b) are identical, the left hand sides are too:

$$(v_r - u)\frac{dr}{du} = -(v_l + u)\frac{dl}{du} \tag{9}$$

Moreover, at $t_0 \gg 1$, $i = (v_r + v_l) l r$, so that

$$l = \frac{i}{(v_r + v_l) r} \tag{10}$$

Substituting (10) into (9), we have

$$\frac{dr}{du}\left[(v_r - u) - \frac{i}{v_r + v_l}\frac{(v_l + u)}{r^2}\right] = 0 \tag{11}$$

Thus the solutions are

$$r = \sqrt{\frac{i}{v_r + v_l}}\sqrt{\frac{v_l t + x}{v_r t - x}} \tag{12}$$

and, using (10),

$$l = \sqrt{\frac{i}{v_r + v_l}}\sqrt{\frac{v_r t - x}{v_l t + x}} \tag{13}$$

It is important to note that Eqs. (12) and (13) fail to satisfy boundary conditions (5c) and (5d). For $v_r = v_l$, it was shown by Mansfield [6] and by Point and Villers [7] that the assumption of the sole dependence of l and r on u (affine growth) fails near

the crystal edges $x=-ht$ and $x=+ht$ if $h<v$. Therefore, we require correction terms that are significant only near the edges. In the steady state we expect these to be functions of the distance from the edge, and to be significant only over distances much smaller than ht.

$$r=\sqrt{\frac{i}{v_r+v_l}}\sqrt{\frac{v_lt+x}{v_rt-x}}+f_1(x+h_lt)+f_2(-x+h_rt) \tag{14a}$$

$$l=\sqrt{\frac{i}{v_r+v_l}}\sqrt{\frac{v_rt-x}{v_lt+x}}+f_3(x+h_lt)+f_4(-x+h_rt) \tag{14b}$$

Here, f_1 and f_3 are significant only near the left edge $x=-h_lt$, while f_2 and f_4 are significant only near the right edge $x=h_rt$. We refer to the last two terms of Eqs. (14a) and (14b) as edge terms, since only these terms contain the substrate edge velocities h_r and h_l. The edge terms and their determination below are similar to those described by Mansfield [6] except for the very important difference that r and l functions are not symmetrically related because of the asymmetry of the growth face: $r(x,t)\neq l(-x,t)$. Since the edge terms are also asymmetric, we have to define them independently for the densities of right and left steps. Substituting

$$\xi_1=x+h_lt \tag{15a}$$

$$\xi_2=-x+h_rt \tag{15b}$$

we have

$$r=\sqrt{\frac{i}{v_r+v_l}}\sqrt{\frac{v_lt+x}{v_rt-x}}+f_1(\xi_1)+f_2(\xi_2) \tag{16a}$$

$$l=\sqrt{\frac{i}{v_r+v_l}}\sqrt{\frac{v_rt-x}{v_lt+x}}+f_3(\xi_1)+f_4(\xi_2) \tag{16b}$$

Differentiating (16a) and (16b) gives

$$\frac{\partial r}{\partial x}=\frac{1}{2}\sqrt{\frac{i}{v_r+v_l}}\sqrt{\frac{v_rt-x}{v_lt+x}}\frac{(v_r+v_l)t}{(v_rt-x)^2}+f_1'(\xi_1)-f_2'(\xi_2) \tag{17}$$

$$\frac{\partial r}{\partial t}=-\frac{1}{2}\sqrt{\frac{i}{v_r+v_l}}\sqrt{\frac{v_rt-x}{v_lt+x}}\frac{(v_r+v_l)x}{(v_rt-x)^2}+h_lf_1'(\xi_1)+h_rf_2'(\xi_2) \tag{18}$$

$$\frac{\partial l}{\partial x}=-\frac{1}{2}\sqrt{\frac{i}{v_r+v_l}}\sqrt{\frac{v_lt+x}{v_rt-x}}\frac{(v_r+v_l)t}{(v_lt+x)^2}+f_3'(\xi_1)-f_4'(\xi_2) \tag{19}$$

$$\frac{\partial l}{\partial t}=\frac{1}{2}\sqrt{\frac{i}{v_r+v_l}}\sqrt{\frac{v_lt+x}{v_rt-x}}\frac{(v_r+v_l)x}{(v_lt+x)^2}+h_lf_3'(\xi_1)+h_rf_4'(\xi_2) \tag{20}$$

Using (16)–(18) in (5a), and (16), (19), (20) in (5b), we have

$$\begin{aligned}&\frac{1}{2}\sqrt{\frac{i}{v_r+v_l}}\sqrt{\frac{v_rt-x}{v_lt+x}}\frac{(v_r+v_l)}{(v_rt-x)}+(h_l+v_r)f_1'(\xi_1)\\&+(h_r-v_r)f_2'(\xi_2)=-(v_r+v_l)\times\left[\sqrt{\frac{i}{v_r+v_l}}\sqrt{\frac{v_lt+x}{v_rt-x}}(f_3(\xi_1)\right.\\&+f_4(\xi_2))+\sqrt{\frac{i}{v_r+v_l}}\sqrt{\frac{v_rt-x}{v_lt+x}}(f_1(\xi_1)+f_2(\xi_2))+\{(f_1(\xi_1)\\&\left.+f_2(\xi_2))(f_3(\xi_1)+f_4(\xi_2))\}\right]\end{aligned} \tag{21a}$$

$$\begin{aligned}&\frac{1}{2}\sqrt{\frac{i}{v_r+v_l}}\sqrt{\frac{v_lt+x}{v_rt-x}}\frac{(v_r+v_l)}{(v_lt+x)}+(h_l-v_l)f_3'(\xi_1)\\&+(h_r+v_l)f_4'(\xi_2)=-(v_r+v_l)\times\left[\sqrt{\frac{i}{v_r+v_l}}\sqrt{\frac{v_lt+x}{v_rt-x}}(f_3(\xi_1)\right.\\&+f_4(\xi_2))+\sqrt{\frac{i}{v_r+v_l}}\sqrt{\frac{v_rt-x}{v_lt+x}}(f_1(\xi_1)+f_2(\xi_2))+\{(f_1(\xi_1)\\&\left.+f_2(\xi_2))(f_3(\xi_1)+f_4(\xi_2))\}\right]\end{aligned} \tag{21b}$$

Omitting the first term on the left hand side of Eqs. (21a) and (21b), which is in both cases $O(1/t)$ and is negligible at large times, we have

$$\begin{aligned}&(h_l+v_r)f_1'(\xi_1)+(h_r-v_r)f_2'(\xi_2)=-(v_r+v_l)\\&\times\left[\sqrt{\frac{i}{v_r+v_l}}\sqrt{\frac{v_lt+x}{v_rt-x}}(f_3(\xi_1)+f_4(\xi_2))\right.\\&+\sqrt{\frac{i}{v_r+v_l}}\sqrt{\frac{v_rt-x}{v_lt+x}}(f_1(\xi_1)+f_2(\xi_2))+\{(f_1(\xi_1)\\&\left.+f_2(\xi_2))(f_3(\xi_1)+f_4(\xi_2))\}\right]\end{aligned} \tag{22a}$$

$$\begin{aligned}&(h_l-v_l)f_3'(\xi_1)+(h_r+v_l)f_4'(\xi_2)=-(v_r+v_l)\\&\times\left[\sqrt{\frac{i}{v_r+v_l}}\sqrt{\frac{v_lt+x}{v_rt-x}}(f_3(\xi_1)+f_4(\xi_2))\right.\\&+\sqrt{\frac{i}{v_r+v_l}}\sqrt{\frac{v_rt-x}{v_lt+x}}(f_1(\xi_1)+f_2(\xi_2))+\{(f_1(\xi_1)\\&\left.+f_2(\xi_2))(f_3(\xi_1)+f_4(\xi_2))\}\right]\end{aligned} \tag{22b}$$

Near the left edge $x=-h_lt$, $\xi_1\to 0$, $\xi_2\to(h_l+h_r)t$, so all the functions f_i with argument ξ_2 and their derivatives with argument ξ_2 are negligible. Thus, we can rewrite Eqs. (22) in

the following manner:

$$(h_l + v_r)f_1'(\xi_1) = -(v_r + v_l) \times \left[\sqrt{\frac{i}{v_r + v_l}} \sqrt{\frac{v_l - h_l}{v_r + h_l}} f_3(\xi_1) + \sqrt{\frac{i}{v_r + v_l}} \sqrt{\frac{v_r + h_l}{v_l - h_l}} f_1(\xi_1) + f_1(\xi_1) f_3(\xi_1) \right] \tag{23a}$$

$$(h_l - v_l)f_3'(\xi_1) = -(v_r + v_l) \times \left[\sqrt{\frac{i}{v_r + v_l}} \sqrt{\frac{v_l - h_l}{v_r + h_l}} f_3(\xi_1) + \sqrt{\frac{i}{v_r + v_l}} \sqrt{\frac{v_r + h_l}{v_l - h_l}} f_1(\xi_1) + f_1(\xi_1) f_3(\xi_1) \right] \tag{23b}$$

Since the right hand sides of Eqs. (23a) and (23b) are equal, $(h_l + v_r)f_1'(\xi_1) = (h_l - v_l)f_3'(\xi_1)$, and

$$f_3 = \frac{h_l + v_r}{h_l - v_l} f_1 \tag{24}$$

The integration constant in (24) is zero because both functions are zero except in the narrow region of $\xi_1 \to 0$.

Inserting (24) into Eq. (23a), we have:

$$\frac{df_1}{d\xi_1} = \frac{v_r + v_l}{v_l - h_l} f_1^2 \tag{25}$$

After integration this gives

$$f_1 = \frac{h_l - v_l}{(v_r + v_l)y + C_1(v_l - h_l)} \tag{26}$$

where C_1 is an integration constant. Substituting (26) into (24), we have for f_3:

$$f_3 = \frac{h_l + v_r}{(v_r + v_l)y + C_1(v_l - h_l)} \tag{27}$$

Repetition of the above treatment of Eqs. (22a) and (22b) near the right edge $x = h_r t$, $\xi_1 \to (h_l + h_r)t$, $\xi_2 \to 0$, results in the following expressions for functions f_2 and f_4.

$$f_2 = \frac{h_r + v_l}{(v_r + v_l)y + C_2(v_l + h)} \tag{28}$$

$$f_4 = \frac{h_r - v_r}{(v_r + v_l)y + C_2(v_l + h)} \tag{29}$$

where C_2 is another integration constant.

Combining parts (16), (26)–(29) of the solution, we have as a result

$$r = \sqrt{\frac{i}{v_r + v_l}} \sqrt{\frac{v_l t + x}{v_r t - x}} + \frac{h_l - v_l}{(v_r + v_l)(x + h_l t) + C_1(v_l - h_l)} + \frac{h_r + v_l}{(v_r + v_l)(-x + h_r t) + C_2(v_l + h_r)} \tag{30a}$$

$$l = \sqrt{\frac{i}{v_r + v_l}} \sqrt{\frac{v_r t - x}{v_l t + x}} + \frac{h_l + v_r}{(v_r + v_l)(x + h_l t) + C_1(v_l - h_l)} + \frac{h_r - v_r}{(v_r + v_l)(-x + h_r t) + C_2(v_l + h_r)} \tag{30b}$$

To find constants C_1 and C_2, we use the boundary conditions (5c) and (5d) at large values of time:

$$r(-h_l t) = \sqrt{\frac{i}{v_r + v_l}} \sqrt{\frac{v_l - h_l}{v_r + h_l}} - \frac{1}{C_1} = 0 \tag{31a}$$

$$l(h_r t) = \sqrt{\frac{i}{v_r + v_l}} \sqrt{\frac{v_r - h_r}{v_l + h_r}} - \frac{1}{C_2} \frac{v_r - h_r}{v_l + h_r} = 0 \tag{31b}$$

$$C_1 = \sqrt{\frac{v_r + v_l}{i}} \sqrt{\frac{v_r + h_l}{v_l - h_l}} \tag{32}$$

$$C_2 = \sqrt{\frac{v_r + v_l}{i}} \sqrt{\frac{v_r - h_r}{v_l + h_r}} \tag{33}$$

Finally, inserting (32) and (33) into (30a) and (30b) we obtain:

$$r = \sqrt{\frac{i}{v_r + v_l}} \sqrt{\frac{v_l t + x}{v_r t - x}} + \frac{h_l - v_l}{(v_r + v_l)(x + h_l t) + \sqrt{(v_r + v_l)/i}\sqrt{(v_r + h_l)(v_l - h_l)}} + \frac{h_r + v_l}{(v_r + v_l)(-x + h_r t) + \sqrt{(v_r + v_l)/i}\sqrt{(v_r - h_r)(v_l + h_r)}} \tag{34a}$$

$$l = \sqrt{\frac{i}{v_r + v_l}} \sqrt{\frac{v_r t - x}{v_l t + x}} + \frac{h_l + v_r}{(v_r + v_l)(x + h_l t) + \sqrt{(v_r + v_l)/i}\sqrt{(v_r + h_l)(v_l - h_l)}} + \frac{h_r - v_r}{(v_r + v_l)(-x + h_r t) + \sqrt{(v_r + v_l)/i}\sqrt{(v_r - h_r)(v_l + h_r)}} \tag{34b}$$

3.2. Shape of the growth front

The profile of the growth front at time t is obtained by integration of the differential Eq. (2):

$$y(x,t) = b \int_{-v_l t}^{x} \left[l(x',t) - r(x',t) \right] dx' \tag{35a}$$

The value of y at x on the left-hand side of the growth front is calculated by counting all the steps between the left limit $-v_l t$ and x at a given time, and adding $+b$ for each left-moving step and $-b$ for each right-moving step. By analogy, for the right-hand side of the growth front

$$y(x,t) = b\int_{x}^{v_r t}\left[r(x',t)-l(x',t)\right]\mathrm{d}x' \tag{35b}$$

It must be underlined that we integrate between $-v_l t$ and $+v_r t$ irrespective of whether the growth front is or is not curtailed by other faces. If the velocity of the substrate edges is smaller than that of the growth steps v, the actual growth face limits will be $-h_l t$ and $+h_r t$. The blanket use of integration limits $-v_l t$ and $+v_r t$ is justified because, as is shown in Appendix A, for a finite size crystal, the growth profile is unaffected by the proximity of the crystal edges.

According to (34a) and (34b), the integrand function in (35a) is

$$\begin{aligned} l-r = {} & \sqrt{\frac{i}{v_r+v_l}}\left(\sqrt{\frac{v_r t-x}{v_l t+x}}-\sqrt{\frac{v_l t+x}{v_r t-x}}\right) \\ & + \frac{v_r+v_l}{(v_r+v_l)(x+h_l t)+\sqrt{(v_r+v_l)/i}\sqrt{(v_r+h_l)(v_l-h_l)}} \\ & - \frac{v_r+v_l}{(v_r+v_l)(-x+h_r t)+\sqrt{(v_r+v_l)/i}\sqrt{(v_r-h_r)(v_l+h_r)}} \end{aligned} \tag{36}$$

Upon integration the last two terms of Eq. (36) scale as $\ln t$, while the first term scales as t. Thus, at large times we can neglect the last two terms and assume

$$l-r = \sqrt{\frac{i}{v_r+v_l}}\left(\frac{(v_r-v_l)t-2x}{\sqrt{(v_r t-x)(v_l t+x)}}\right) \tag{37}$$

The last two terms of Eq. (36) are the edge terms, already defined in relation to Eqs. (14), since only these terms contain the substrate edge velocities h_r and h_l. It should be borne in mind that even if $v_r=h_r$ and $v_l=h_l$, there is a difference in integrands (36) and (37). This difference will be called the non-elliptical deviation. The substrate edge effect ($h<v$) contributes to the overall non-elliptical deviation. The validity of the switch from integrand (36) to integrand (37) in the reconstruction of the growth shape is elaborated in the Appendix A.

After trivial integration we have for the growth front profile

$$\frac{y}{t} = 2b\sqrt{\frac{i}{v_r+v_l}}\sqrt{\left(v_r-\frac{x}{t}\right)\left(v_l+\frac{x}{t}\right)} \tag{38}$$

which gives, in the standard quadratic form for time-independent coordinates $X=x/t$ and $Y=y/t$ (because the growth of the crystal is affine):

$$\left[\frac{X+(v_l-v_r)/2}{(v_l+v_r)/2}\right]^2+\left[\frac{Y}{b\sqrt{i(v_r+v_l)}}\right]^2 = 1 \tag{39}$$

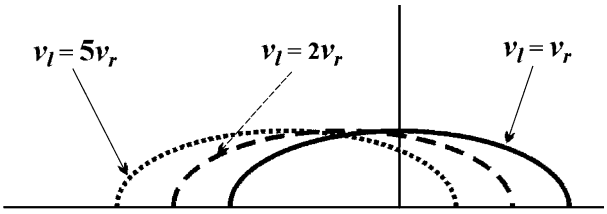

Fig. 3. Three growth fronts given by Eq. (39) for the ratio $ib^2/(v_r+v_l)=0.05$ and $v_{aver}=3$, with different v_l/v_r ratios.

This is the equation of an ellipse with the centre shifted by $-(v_l-v_r)/2$ along the X-axis. Let us compare the ellipse (39) with the Mansfield ellipse:

$$\left[\frac{x}{v}\right]^2+\left[\frac{y}{b\sqrt{2iv}}\right]^2 = 1 \tag{40}$$

In the latter case, the axial ratio R defining the curvature of the growth face is determined only by the ratio of initiation and propagation rates:

$$R = \frac{b\sqrt{2iv}}{v} = \sqrt{2}b\sqrt{\frac{i}{v}}. \tag{41}$$

For the ellipse given by Eq. (39):

$$R = \sqrt{2}b\sqrt{\frac{i}{(v_r+v_l)/2}} \tag{42}$$

Here, the axial ratio is also determined solely by the ratio of initiation rate and the average velocity of propagation in the right and left directions. Thus the only difference in the shape of symmetric and asymmetric faces is the shift of the centre of the ellipse along the x-axis in the latter case. This also means that the maximum of the growth front is no longer at the centre of the substrate, but rather is located closer to one of its edges. The larger the difference in rates of propagation of the right and left steps, the larger is the shift. These features are illustrated in Fig. 3.

4. Discussion and conclusion

In the above, we have solved the growth equation for a lateral crystal face for which the step propagation rate is not only slow but also unequal in the right and left direction. The main result is that, as in the symmetrical case, such growth results in an elliptical $y(x)$ profile of the growth face; however, the centre of the ellipse is shifted along the x-axis in the direction of fast step propagation. As in Mansfield's treatment of symmetric growth [6], we find that, for long time t, the elliptical profile is a good approximation even in the case where the substrate spreading rate h is less than the step spreading rate v (Appendix A). For very small crystals, typically below 0.1 μm, a correction is required near the corners. However, since such small crystals contain a small number of nucleation sites, the validity of the entire continuum approach becomes questionable. Thus, where the theory applies, correction terms are not required.

Since faces are curved when the average step propagation distance is no larger than several stem widths, this type of crystal growth is at the borderline between nucleated and rough-surface type. Actually, as was noticed by Frank himself [8], as well as by Sadler [4] and Mansfield [6], a pure nucleation model cannot be used to describe a curved growth front. Much in agreement with this judgment, an alternative derivation of the growth profile of lamellar polymer crystals, also based on Eqs. (1), has been proposed by Point and Villers [7]. According to these authors, their equations are equally applicable to the secondary nucleation and the rough surface growth mechanism. In actual fact, the curved growth face shape obtained by Point and Villers is very close to that obtained by Mansfield.

The mathematical treatment of curved faces growing asymmetrically, developed in the present work, opens the way for interpretation of a wide range of polymer crystal habits. The solution of the growth profile given here is for the simple square lattice, and is thus directly applicable only to crystals with a primitive tetragonal crystal unit cell. The next step is to transpose accurately the equations derived here to 2D lattices reflecting the crystallography of individual polymer. This work is now in progress, starting with the specific examples of polyethylene, poly(vinylidene fluoride) and poly(ethylene oxide) [19].

Acknowledgements

The authors are grateful for financial support by the Engineering and Physical Research Council.

Appendix A

In the reconstruction of the shape of the growth front one should clarify two issues arising in conjunction with Eqs. (35). The first one is the validity of neglecting the edge terms in integrand (36) in the reconstruction of the growth of a real crystal. This is connected to the effect of the moving substrate edges $-h_l t$ and $h_r t$. The second issue is the choice of integration limits and its effect on the shape of the growth front.

A.1. Neglect of edge terms

Regarding the first issue, the problem is that before integration of (35) we do not know whether we are allowed to neglect the edge terms and replace the integrand (36) by (37), thus neglecting the substrate edge effect. We will show below that inclusion of the edge terms indeed makes no difference to the shape of the crystals of observable size.

For the sake of simplicity we switch to the case of symmetric growth with $v_r = v_l$. We determine the non-elliptical deviation for this case; even though Mansfield neglected the edge terms in his original work [6], the extent of the deviation of the growth front from the elliptical shape was not elaborated.

Converted to the symmetric case, Eqs. (36) and (37) become Eqs. (A1) and (A2), respectively:

$$l-r = -2\sqrt{\frac{i}{2v}}\left(\frac{x}{\sqrt{v^2t^2-x^2}}\right) + 2v\left[\frac{1}{(x+ht)+\sqrt{(v^2-h^2)/2iv}} - \frac{1}{(-x+ht)+\sqrt{(v^2-h^2)/2iv}}\right] \tag{A1}$$

$$l-r = -2\sqrt{\frac{i}{2v}}\left(\frac{x}{\sqrt{v^2t^2-x^2}}\right) \tag{A2}$$

In Fig. A1 the function $|l-r|$ is shown for the following cases: (1) $v=h$, correction functions neglected (Eq. (A2)); (2) $v=h$, correction functions applied (Eq. (A1)); (3) $v=0.7h$, correction functions applied, the difference with the first case is due to the boundary effect with the contribution of the substrate edge effect. The difference between curves 1 and 2, which is the cause of the non-elliptical shape deviation, scales as $1/t$ and becomes negligible with time, as one can see comparing Fig. A1(a) and (b). This difference, which does not involve the substrate edge effect, disappears with time very rapidly. The distortion of the ends of curve 3 is due to the conditions (4a) and (4b), which require that functions r and l be zero at the substrate edges $-ht$ and $+ht$, respectively. The difference between curves 3 and 1 disappears somewhat more slowly; nevertheless, as will be shown in Fig. A2, it ceases to have a noticeable effect once the crystals reach ca. 0.1 μm. In plotting Fig. A1 we used values of propagation and initiation rates, which are typical for the growth of real polymer crystals.

We now turn to the construction of the growth front $y(x,t)$, taking its left hand side as an example. For the cases pertaining to curves 1 or 2 of Fig. A1, the value of y at x is equal to the area under these curves between $-vt$ and x. The results of integration of (35) with integrands (A1) and (A2) are compared in Fig. A2. The calculation was performed using the same kinetic parameters as in Fig. A1. Integration of curve 1 gives the Mansfield ellipse. The other three growth profiles in Fig. A2 are obtained by integrating curves 3a, 3b and 3c.

It is clear from Fig. A2 that for crystals larger than ca. 0.1 μm there is indeed no need to apply the correction functions in the reconstruction of the growth front; the use of integrand (37) in Eqs. (35a) and (35b) is thus justified. For smaller crystals the validity of the entire approach becomes dubious anyway, due to the small number of sites involved.

A.2. Integration limits

The question of integration limits in the construction of the growth profile $y(x)$ (Eqs. (35a) and (35b)) requires some consideration. As mentioned before, when the propagation rate of the crystal edges is smaller than that of the moving steps, the real growth face exists only between $x_l = -h_l t$ and $x_r = +h_r t$. Accordingly, it would seem rational to use x_l as the lower integration limit in (35a) and x_r as the upper integration limit in

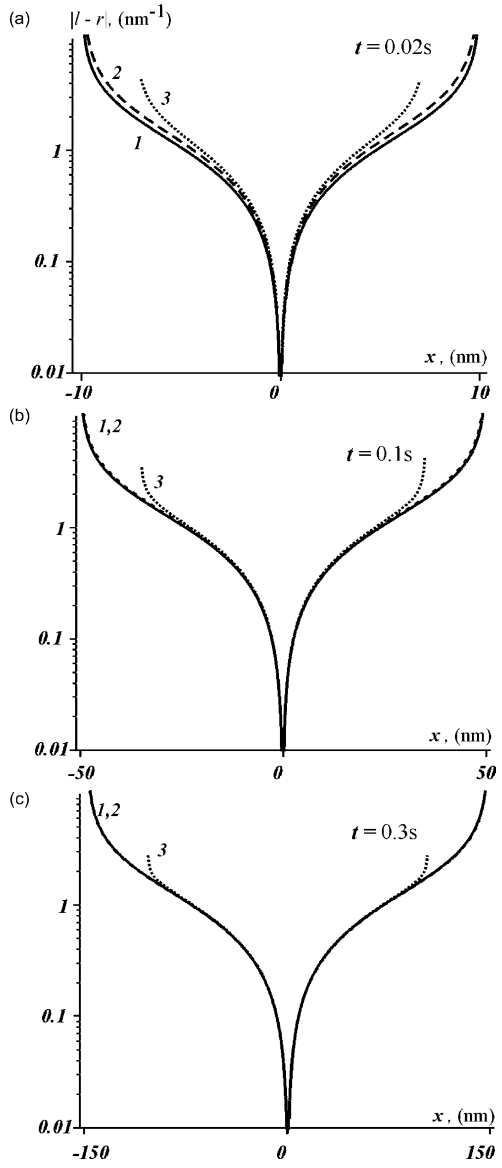

Fig. A1. The absolute value of difference of right-moving and left-moving step densities for the symmetrical growing plane with $v=500$ nm/s. $ib^2/(v_r+v_l)=0.2$. Curve 1: $h=v$, correction functions neglected. Curve 2 (dashed line): $h=v$, correction functions applied. Curve 3 (dotted line): $h=0.7\,v$, correction functions applied. Graphs are plotted at times (a) $t=0.02$ s, (b) 0.1 s and (c) 0.3 s.

(35b). However, this would mean that the counting of steps starts from zero at $x_l=-h_l t$ and $x_r=+h_r t$, automatically giving this points a zero value of y and thus shifting the reference plane relative to the original x-axis. This was the approach adopted in Ref. [6]. Furthermore, since in the asymmetric case the propagation rates of the right and left substrate edges could differ, this would additionally lead to a tilt of the reference plane and to a variety of ambiguities when reconstructing the entire shape of a single crystal.

Given that for finite crystals the truncation effect on the shape of the growth front is negligible (Fig. A2), we decided to perform the integration within the entire range between

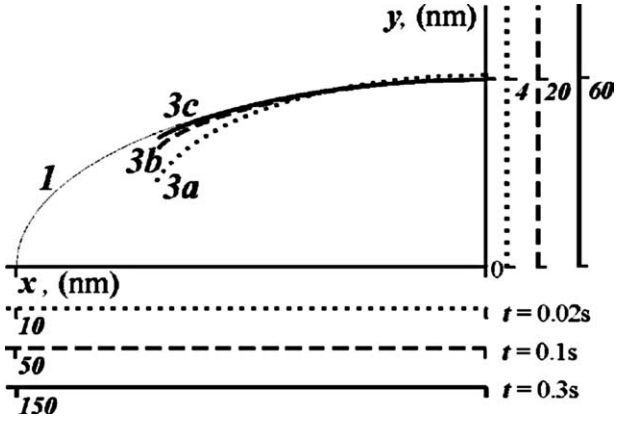

Fig. A2. Calculated growth profiles obtained by using in Eq. (35) different integrands. Curve 1: the integrand is (A2) (curve 1 in Fig. 3). Curves 3a, 3b and 3c: the integrand is (A1) with the parameters equal to those as for curves 3a, 3b, 3c in Fig. A1.

$x=-v_l t$ and $x=v_r t$, even if $h_l<v_l$ and $h_r<v_r$. The fact that in crystals of visible size the edge effects can be neglected implies that the value of $y(x)$ will be determined only by the nuclei formed in the vicinity of x. Therefore, the fact that the growth front physically does not exist between $-v_l t$ and $-h_l t$, and between $+h_r t$ and $+v_r t$, does not prevent us from using the integration limits $-v_l t$ and $+v_r t$. In this way we avoid the problems of shifting and tilting reference plane.

In the reconstruction of the growth front we switch between Eqs. (35a) and (35b) at the point $x=(v_r-v_l)/2$, where the function $|l-r|$ is zero. The boundary velocities $h_l<v_l$ near the left edge and $h_r<v_r$ near the right edge are taken into account simply by cutting the growth front at the points $x=-h_l t$ and $x=h_r t$.

References

[1] Keith HD. J Appl Phys 1964;35:3115.
[2] Khoury F. Faraday Discuss Chem Soc 1979;68:404.
[3] Sadler DM. Polymer 1983;24:1401.
[4] Sadler DM, Gilmer GH. Polym Commun 1987;28:243.
[5] Toda A. Polymer 1991;32:771.
[6] Mansfield ML. Polymer 1988;29:1755.
[7] Point JJ, Villers D. J Cryst Growth 1991;114:228.
[8] Frank FC. J Cryst Growth 1974;22:233.
[9] Organ SJ, Keller A, Hikosaka M, Ungar G. Polymer 1996;37:2517.
[10] Ungar G, Mandal PK, Higgs PG, de Silva DSM, Boda E, Chen CM. Phys Rev Lett 2000;85:4397.
[11] Putra EGR, Ungar G. Macromolecules 2003;36:3812.
[12] Putra EGR, Ungar G. Macromolecules 2003;36:5214.
[13] Ungar G, Putra EGR. Macromolecules 2001;34:5180.
[14] Ungar G, Putra EGR, de Silva DSM, Shcherbina MA, Waddon AJ. Adv Polym Sci; 180:45.
[15] Seto T. Rep Prog Polym Phys Jpn 1964;7:67.
[16] Organ SJ, Keller AJ. Mater Sci 1985;20:1571.
[17] Tanzawa Y, Toda A. Polymer 1996;37:1621.
[18] Toda A. Faraday Discuss 1993;95:129.
[19] Shcherbina MA, Ungar G. In preparation.